

Spontaneous radiative dissociation of the second bound state of positronium hydride

Takuma Yamashita ^{*}


*Institute for Excellence in Higher Education, Tohoku University, Sendai, Miyagi 980-8576, Japan
and Department of Chemistry, Tohoku University, Sendai, Miyagi 980-8578, Japan*

Emiko Hiyama

*Department of Physics, Tohoku University, Sendai, Miyagi 980-8578, Japan
and Nishina Center, RIKEN, Wako, Saitama 351-0198, Japan*

Daisuke Yoshida  and Masanori Tachikawa

Quantum Chemistry Division, Yokohama City University, Yokohama 236-0027, Japan

 (Received 29 July 2021; revised 4 January 2022; accepted 5 January 2022; published 20 January 2022)

The spontaneous radiative dissociation spectrum of the second bound state of positronium hydride (PsH) located just below the $H(2p) + Ps(2p)$ threshold energy is investigated by the variational and complex coordinate rotation methods. Convergence of the transition rates is examined in both length and velocity gauges. The spectrum indicates that the primary channel of radiative dissociation is the transition into the continuum of $H(1s) + Ps(2p)$, and the secondary one is that into the $H(2p) + Ps(1s)$ continuum. Radiative transition to the resonance state located close to the second bound state is found to exist. The total rate of the radiative dissociation is found to be $9.1(2) \times 10^8 \text{ s}^{-1}$.

DOI: [10.1103/PhysRevA.105.012814](https://doi.org/10.1103/PhysRevA.105.012814)

I. INTRODUCTION

Optical transitions of the hydrogen atom and its related systems are of importance in understanding stellar radiation and have attracted considerable attention in astrophysics [1–5]. The negative hydrogen ion (H^-), which usually refers to the $1s^2$ ground state ($^1S^e$) located below the $H(1s) + e^-$ dissociation threshold energy, is known to play an important role in stellar absorption spectra, or opacity [1,6–9], and several methods are dedicated to accurate prediction of the photodetachment processes of H^- [10–14]. Here, the term symbol represents $^{2s+1}L^\Pi$ where s denotes the total spin quantum number of electrons, L total orbital angular momentum quantum number, and $\Pi = \pm 1$ spatial parity e (even, $\Pi = 1$) or o (odd, $\Pi = -1$). The optical transitions of the hydrogen molecule also contribute to the opacity, and in addition, the decay of their dissociative states produces hot hydrogen atoms which play an important role in interstellar reaction kinetics.

Although most of the electronically excited states of these species are unstable against the autoionization, some of them are known to be stable against such nonradiative dissociation. $H^-(2p^2\ ^3P^e)$ is known as the second bound state, with 0.0096 eV binding energy, below the $H(2p) + e^-$ dissociation threshold energy [15–17]. The two electrons in $H^-(2p^2\ ^3P^e)$ are doubly excited in a spin triplet ($S = 1$) and possess the total orbital angular momentum $L = 1$ in even parity ($\Pi = 1$). The corresponding vector \mathbf{L} is composed of the angular momentum between the two electrons, \mathbf{l}_1 , and the angular

momentum between the center of mass of the two electrons and the proton, \mathbf{l}_2 . The conditions $L = 1$ and $\Pi = 1$ only allow $l_1 = l_2 \geq 1$. As the $H(1s) + e^-$ continuum has $\Pi = (-1)^L$ owing to the s orbital of the H atom, $H^-(^3P^e)$ has no overlapping continuum (under the LS -coupling approximation), and thus the autoionization of $H^-(^3P^e)$ is prohibited. A similar bound state that has doubly excited electrons but does not undergo autoionization is also known in the H_2 molecule, as Σ^- bound states that are located below the $H(2p) + H(2p)$ dissociation threshold energy [18–20].

As the two H atoms form a bound state, the H atom and a positronium (Ps; a bound state of an electron and a positron) also form a bound state, called positronium hydride (PsH) [21–32]. PsH can be regarded as a hydrogen-like molecule in which one of the H_2 protons is replaced by the positron (e^+) or as a proton-lepton system in which H^- binds itself by the positron. Positrons are known to be abundant in the galaxy, and astrophysical observation suggests that most positrons form Ps before being annihilated [33]. Thus, the optical transitions of the PsH system might also contribute to stellar spectra.

Although the bound state of PsH usually refers to the $^2S^e$ state, there exists a second bound state in $^{2,4}S^o$ that has doubly excited electrons but does not undergo nonradiative dissociation [34]. Regarding the term symbol of $^{2s+1}L^\Pi$ of PsH, s denotes the total spin quantum number of leptons. The ground state of PsH ($^2S^e$) has spin singlet electrons and a positron, which gives $s = 1/2$. $PsH(^{2,4}S^o)$ has spin triplet electrons (hence $s = 1/2$ or $3/2$) and 0.019 eV binding energy against the lowest dissociation threshold of $H(2p) + Ps(2p)$. The odd parity ($\Pi = -1$) with the total orbital angular

^{*}tyamashita@tohoku.ac.jp

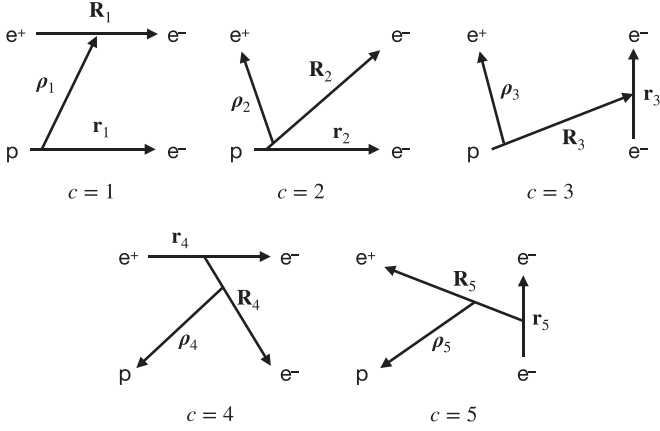


FIG. 2. Jacobi coordinate systems for PsH.

velocity gauge,

$$\mathbf{d}(\theta) = -\frac{e^{-i\theta}}{E_\gamma} \left(\frac{1}{\mu_{pe^-}} \nabla_{p \rightarrow e^-} + \frac{1}{\mu_{e^+e^-}} \nabla_{e^+ \rightarrow e^-} \right), \quad (7)$$

where μ_{ij} is the reduced mass between particles i and j , and $\nabla_{i \rightarrow j}$ is the differential operator associated with $\mathbf{r}_{i \rightarrow j}$.

$d\Gamma_\gamma/dE_\gamma$ would give the same results in the length and velocity gauges if the $\Psi_i(\theta)$ and $\psi_n(\theta)$ were exact. However, as described above, the PsH($2,4P^e$) continuum wave function in principle involves infinitely many dissociation channels, which makes it difficult to construct the exact scattering wave function. In this work, $\Psi_i(\theta)$ and $\psi_n(\theta)$ are calculated by the variational method for energy and are expanded in terms of the square integrable functions to satisfy

$$\langle \bar{\Psi}_i(\theta) | H(\theta) | \Psi_i(\theta) \rangle = E_i(\theta) \quad (8)$$

and

$$\langle \bar{\psi}_n(\theta) | H(\theta) | \psi_m(\theta) \rangle = E_n(\theta) \delta_{nm}. \quad (9)$$

Therefore, the discrepancy between $d\Gamma_\gamma/dE_\gamma$ in the length and velocity gauges are an indicator of the numerical accuracy.

B. Bound state

For the description of the bound-state wave function, Ψ_i , we consider the five Jacobi coordinate systems $\{\mathbf{r}_c, \mathbf{R}_c, \boldsymbol{\rho}_c\}$ ($c = 1-5$) illustrated in Fig. 2 and their electron-permuted counterparts. As described above, the angular momentum of the interparticle motion in PsH($2,4S^o$) is not zero. $\Psi_i(\theta)$ can be expanded in terms of Gaussian functions and spherical harmonics as follows:

$$\begin{aligned} \Psi_i(\theta) = & \sum_c \sum_{ijk} (1 - \mathcal{P}) C_{cijk}(\theta) r_c R_c \rho_c \\ & \times \exp(-a_i r_c^2 - A_j R_c^2 - \alpha_k \rho_c^2) \\ & \times \exp(-\sigma_c^{(1)} \sqrt{a_i A_j} \mathbf{r}_c \cdot \mathbf{R}_c \\ & - \sigma_c^{(2)} \sqrt{A_j \alpha_k} \mathbf{R}_c \cdot \boldsymbol{\rho}_c - \sigma_c^{(3)} \sqrt{\alpha_k a_i} \boldsymbol{\rho}_c \cdot \mathbf{r}_c) \\ & \times [[Y_1(\hat{\mathbf{r}}_c) \otimes Y_1(\hat{\mathbf{R}}_c)]_1 \otimes Y_1(\hat{\boldsymbol{\rho}}_c)]_{LM_L}, \end{aligned} \quad (10)$$

where $L = M_L = 0$ for S state, \mathcal{P} is the permutation operator for two electrons, and c denotes the corresponding Jacobi coordinate system in Fig. 2. The linear coefficients $C_{cijk}(\theta)$ (complex values depending on θ) are determined by the Rayleigh-Ritz variational principle. $[\dots]$ denotes the linear combination of spherical harmonics with Clebsch-Gordan coefficients as defined in Ref. [41]. Although we do not explicitly write the spin part in Eq. (10), the spin functions configure the triplet state ($S = 1$) for two electrons; therefore, the electron-permuted term is added with a negative sign. The coefficients $\{a_i\}$, $\{A_j\}$, $\{\alpha_k\}$ are chosen to range from 0.001 to 3000 according to their geometric progression. Although each of the basis functions involves only Y_1 functions, the use of several sets of basis functions written in different coordinate systems facilitates description of the interparticle correlation in the bound state [42,43]. For example, the $c = 1$ coordinate system is suitable for describing the $p-e^-$ and e^-e^+ interactions as well as the interaction between these pairs, and $c = 2$ and $c = 3$ are suitable for describing the $(pe^-e^-)e^+$ interaction. $c = 4$ and $c = 5$ provide an auxiliary picture in which the $e^-e^+e^-$ cluster interacts with the proton.

The nonzero $\sigma_c^{(i)}$ introduces the ability to describe the higher angular correlations because

$$\begin{aligned} \exp(-\sigma_c^{(1)} \mathbf{r}_c \cdot \mathbf{R}_c) = & 4\pi \sum_{\lambda=0}^{\infty} \sqrt{2\lambda+1} i_\lambda(\sigma_c^{(1)} r_c R_c) \\ & \times [Y_\lambda(\hat{\mathbf{r}}_c) \otimes Y_\lambda(\hat{\mathbf{R}}_c)]_{00}, \end{aligned} \quad (11)$$

results in the higher order spherical functions. Here i_λ is the modified spherical Bessel function of the first kind. While the $\sigma_c^{(i)}$ can be chosen arbitrarily, the use of basis functions written in different Jacobi coordinates efficiently facilitate the description of the four-body correlation, which allows us to choose $\sigma_c^{(i)}$ from small ranges around zero. In the present work, five kinds of $\sigma_c^{(i)} = 0, \pm 0.04, \text{ and } \pm 0.08$ are used for each basis function.

C. Pseudocontinuum and resonance states

$\psi_n(\theta)$ in Eq. (9) is expanded in terms of Gaussian functions and spherical harmonics as follows:

$$\begin{aligned} \psi_n(\theta) = & \sum_c \sum_{l_c L_c \Lambda_c \lambda_c} \sum_{ijk} (1 - \mathcal{P}) C_{cijk}^{(n)}(\theta) r_c^{l_c} R_c^{L_c} \rho_c^{\lambda_c} \\ & \times \exp(-b_i r_c^2 - B_j R_c^2 - \beta_k (1 + i\varepsilon) \rho_c^2) \\ & \times [[Y_{l_c}(\hat{\mathbf{r}}_c) \otimes Y_{L_c}(\hat{\mathbf{R}}_c)]_{\Lambda_c} \otimes Y_{\lambda_c}(\hat{\boldsymbol{\rho}}_c)]_{L'M'_L}, \end{aligned} \quad (12)$$

where $L' = 1$ and $-1 \leq M'_L \leq L$. The spherical harmonics are chosen to configure even parity, namely, $(-1)^{l_c + L_c + \lambda_c} = 1$. $\{b_i\}$, $\{B_j\}$, and $\{\beta_k\}$ are chosen according to their geometric progression. The ε introduces complex Gaussian functions that are suitable for describing the oscillation behavior of the wave function and contribute to increase the numerical stability of eigenvalue problem. In a way similar to that in the bound-state calculation, $C_{cijk}^{(n)}(\theta)$ is determined by the Rayleigh-Ritz variational principle. The continuum energies, therefore, are discretized as a result of the eigenvalue problem.

The orbital angular momentum quantum numbers l_c, L_c, Λ_c , and λ_c are chosen from the possible combinations of $0 \leq l_c \leq 2$, $0 \leq L_c \leq 2$, $|l_c - L_c| \leq \Lambda_c \leq l_c + L_c$, and

TABLE I. Four-body energy E_i of $\text{PsH}(2^4S^o)$ bound state and expectation values of interparticle distances, listed against the number of basis functions N_b . Here, the proton mass is set to be infinite to facilitate comparison with the previous work [44].

N_b	E_i	$\langle r_{p,e^-} \rangle$	$\langle r_{e^-,e^+} \rangle$	$\langle r_{p,e^+} \rangle$	$\langle r_{e^-,e^-} \rangle$	$\langle r_{p,(e^-,e^+)} \rangle$
34 920	-0.188 189	8.899	12.754	14.301	14.058	10.016
44 850	-0.188 282	8.883	12.740	14.274	14.029	9.997
52 634	-0.188 313	8.870	12.724	14.248	14.006	9.978
Ref. [44]	-0.188 317	8.867	12.722	14.243	14.001	

$0 \leq \lambda_c \leq 2$. As $\text{PsH}(2^4S^o)$ is expected to have a loosely bound structure of $\text{H}(2p) + \text{Ps}(2p)$, the dominant channels of radiative dissociation would be $\text{H}(1s) + \text{Ps}(2p)$ and $\text{H}(2p) + \text{Ps}(1s)$; namely, one of the excited atoms is deexcited, emitting a photon, and the other remains as it is. Thus, basis functions written in the $c = 1$ coordinate system having the angular part of $l_c = 0, L_c = 1, \Lambda_c = 1$, and $\lambda_c = 1$ play a primary role in the description of $\text{H}(n_{\text{H}s}) + \text{Ps}(n_{\text{Ps}p})$. Similarly, those written in the $c = 1$ coordinate system having the angular part of $l_c = 1, L_c = 0, \Lambda_c = 1$, and $\lambda_c = 1$ provide a good description of $\text{H}(2p) + \text{Ps}(1s)$. The $\{b_i\}$ (and $\{B_j\}$) are chosen to range $0.1 \leq b_i^{-2}(B_j^{-2}) \leq 40$ so that the eigenenergies of the dissociation fragments, Ps and H, can be reproduced up to $n \approx 4$ excited states. The $\{\beta_k\}$ for these basis functions are chosen to range $0.1 \leq \beta_k^{-2} \leq 100$ so as to describe the continuum states of $\text{H}(1s) + \text{Ps}(2p)$ and $\text{H}(2p) + \text{Ps}(1s)$ precisely. We typically use 40 parameters of $\{\beta_k\}$ setting $\varepsilon = \pm 0.5$. The set of $\{\beta_k\}$ corresponding to the higher order of the angular part is chosen from the range of $0.1 \leq \beta_k^{-2} \leq 60$ with ε is set to be 0.

Since basis functions written in c coordinate system and having the angular part specified by l_c, L_c, Λ_c , and λ_c have the same physical role in the description of the total wave function. Thus, we call the set of c and $(l_c, L_c, \Lambda_c, \lambda_c)$ ‘‘arrangement channel.’’ We constructed ψ_n with 21 arrangement channels and 61 248 basis functions in total. We examine the convergence of calculation by increasing the number of arrangement channels as well as the number of basis functions.

III. RESULTS AND DISCUSSION

A. Bound state

Table I displays the convergence of the bound-state energy E_i against the number of basis functions N_b . Note that the proton mass is set to be infinite for comparison with the previous work [44]. E_i converges as the number of basis functions increases. Our best bound-state energy value, $-0.188\,313$ a.u., reproduces the best variational value, $-0.188\,317$ a.u. [44], to five digits. Table I also shows the expectation values of inter-particle distances. $r_{i,j}$ denotes the distance between particles i and j , and $r_{i,(jk)}$ denotes the distance between particle i and the center of mass of the pair of particles j and k . As E_i converges, the expectation value of the interparticle distances also converges and shows good agreement with the previous work. The distances between the repulsive particles, $\langle r_{p,e^+} \rangle$ and $\langle r_{e^-,e^-} \rangle$, are approximately 14 a.u., which roughly characterizes the size of this system.

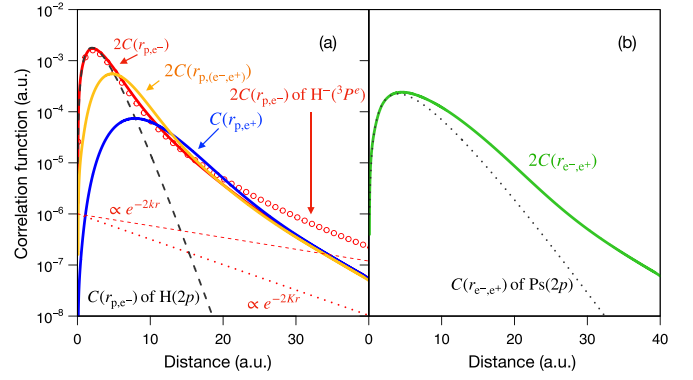


FIG. 3. Interparticle correlation functions (solid lines) of $\text{PsH}(2^4S^o)$ bound state against the distance. (a) Red solid line, $p-e^-$ correlation (multiplied by 2); blue line, $p-e^+$ correlation; orange line, $p-(e^-, e^+)$ correlation (multiplied by 2), where (e^-, e^+) represents the center of mass of e^- and e^+ ; red open circles, $p-e^-$ correlation (multiplied by 2) of $\text{H}^-(3P^e)$; black dashed line, $p-e^-$ correlation of $\text{H}(2p)$. The dotted line is a function of $10^{-6} \exp(-Kr)$ where $K^2/4$ corresponds to the binding energy of $\text{PsH}(2^4S^o)$. The dashed line is $10^{-6} \exp(-kr)$ where $k^2/2$ corresponds to the binding energy of $\text{H}^-(3P^e)$. (b) Green solid line, e^+-e^- correlation of $\text{PsH}(2^4S^o)$; black dotted line, e^+-e^- correlation of $\text{Ps}(2p)$.

In order to see the structure of the $\text{PsH}(2^4S^o)$ bound state, we introduce correlation functions defined as

$$C(r'_{ij}) = \left\langle \Psi_i \left| \frac{\delta(r_{ij} - r'_{ij})}{4\pi r_{ij}^2} \right| \Psi_i \right\rangle, \quad (13)$$

where i and j denote particles $p, e^-,$ or e^+ or the center of mass of a pair of these particles. The correlation function is normalized to unity as $\int C(r'_{ij}) dr'_{ij} = 1$. Figure 3 illustrates correlation functions of the $\text{PsH}(2^4S^o)$ bound state together with those of $\text{H}(2p)$, $\text{H}^-(3P^e)$, and $\text{Ps}(2p)$. Due to the identical nature of the electrons, in the two-electron systems, the correlation functions related to the electron density, $C(r_{p,e^-})$, $C(r_{p,(e^-,e^+)})$, and $C(r_{e^-,e^+})$, are multiplied by 2 so that we can directly compare them with the electron density of $\text{H}(2p)$ and $\text{Ps}(2p)$. Owing to the nonzero interparticle angular momentum, the correlation functions start at zero. As shown in Fig. 3(a), the $p-e^-$ correlation function of $\text{PsH}(2^4S^o)$ has a tail broader than that of $\text{H}(2p)$ whereas the short range ($\lesssim 5$ a.u.) behavior of $\text{PsH}(2^4S^o)$ coincides with that of $\text{H}(2p)$. Similarly, as shown in Fig. 3(b), the e^+-e^- correlation function of $\text{PsH}(2^4S^o)$ has a tail broader than that of $\text{Ps}(2p)$ whereas the short range ($\lesssim 5$ a.u.) behavior coincides with that of $\text{Ps}(2p)$.

It should be noted that the broad tail of the $p-e^-$ correlation function of $\text{PsH}(2^4S^o)$ does not exclude the structure consisting of $\text{Ps}(2p)$ and $\text{H}(2p)$. As indicated in Ref. [44], the shape of the $p-e^-$ correlation function can be well modeled by the $\text{H}(2p) + e^-e^+$ pair. Similarly, the shape of the e^+-e^- correlation function can be well modeled by the $\text{Ps}(2p) + p-e^-$ pair. As we see in Fig. 3, the tail of $2C(r_{p,e^-})$ coincides with those of $2C(r_{p,(e^-,e^+)})$ and $C(r_{p,e^+})$ at the greater distances, which suggests the Ps formation in $\text{PsH}(2^4S^o)$.

The tail of the $p-e^-$ correlation function is shorter than that of $\text{H}^-(3P^e)$. This could be because the attached positron reduces the electron-electron repulsion, causing the electronic size of $\text{PsH}(2^4S^o)$ to shrink, as discussed in the first bound

state of PsH [26,30]. The other explanation can be given by the asymptotic form of the wave function. When the positron and one of the electrons form a Ps at the long distance, the asymptotic form of the p - e^\pm correlation functions should coincide with the analytical form of $\exp(-2Kr)$ where $K = \sqrt{2\varepsilon_b\mu}$ (ε_b , binding energy of PsH($2,4S^o$); μ , reduced mass of Ps and H). Figure 3(a) also shows this asymptotic form as well as that of $H^-(^3P^e)$, $\exp(-2kr)$. Given the fact that the binding energy of PsH($2,4S^o$) is approximately two times larger than that of $H^-(^3P^e)$ and the reduced mass of Ps-H is also two times larger than that of H^-e^- , and K is roughly two times larger than k , which explains the faster decay of the correlation function of PsH($2,4S^o$) than $H^-(^3P^e)$. The p - e^- correlation function of $H^-(^3P^e)$ gradually coincides with the asymptotic form of $\exp(-2kr)$ at the long distance >40 a.u. Similarly, the p - e^\pm correlation functions gradually coincide with the asymptotic form of $\exp(-2Kr)$ at the long distance >40 a.u.

B. Continuum and resonance states

Hereinafter, for calculation of the radiation spectrum, we use the real proton-electron mass ratio $m_p/m_e = 1836.152\,673\,89$ [45], which gives $E_i = -0.188\,237$ a.u. which corresponds to the binding energy of 0.022 123 a.u. Given that the infinite mass condition results in $E_i = -0.188\,313$ a.u. by the present calculation, corresponding to the binding energy of 0.021 906 a.u., the difference between the real proton mass calculation and the infinite proton mass calculation is 0.217 meV.

Because we describe the final states of radiative dissociation in terms of $\psi_n(\theta)$, obtained by the diagonalization of the Hamiltonian [Eq. (9)], the properties of $\psi_n(\theta)$ contribute directly to the radiation spectrum. To investigate the characteristics of $\psi_n(\theta)$ and survey the resonance states embedded in the continuum, we examine the eigenenergies $E_n(\theta)$ for a given rotation angle θ .

Figure 4(a) shows $E_n(\theta)$ for $\theta = 0.16$. Continuum states of $H(nl) + \text{Ps}(n'l')$ are discretized by the use of finite-range basis functions, and their $E_n(\theta)$ values rotate by -2θ owing to the rotation of the kinetic energy operator. The light blue lines of Fig. 4(a) denote the rotated cuts of $H(nl) + \text{Ps}(n'l')$ continuum states, and some $E_n(\theta)$ values below $E_i = -0.188\,237$ clearly lie on these cuts. In particular, the continuum states of $H(1s) + \text{Ps}(n'l')$ for $2 \leq n \leq 5$ and of $H(nl) + \text{Ps}(1s)$ for $2 \leq n \leq 6$ are expected to be well described by the present calculation.

The complex coordinate rotation trajectories of $E_n(\theta)$ reveal a resonance state. Close to E_i , the $2,4P^e$ resonance state is located at resonance energy $-0.199\,502$ (just below the $2,4S^o$ bound-state energy $E_i = -0.188\,237$) with an energy width of 0.001 182. Figure 4(b) shows the trajectories of $E_n(\theta)$ around the complex resonance energy, $E_r - i\Gamma_c/2$. We examined 10 different sets of basis functions (changing the expansion ranges; using the same arrangement channels), increasing θ from 0 to 0.22 by 0.02. All trajectories converge to a unique point on the complex energy plane as θ increases.

For the structural investigation of this resonance state, we introduce expectation values of the interparticle distances:

$$\langle r_{ij} \rangle = \langle \bar{\psi}_n(\theta) | r_{ij} e^{i\theta} | \psi_n(\theta) \rangle. \quad (14)$$

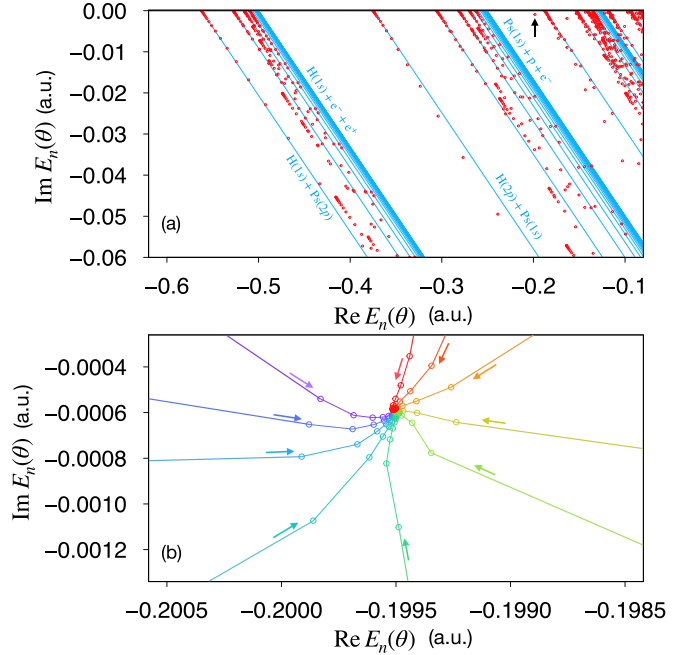


FIG. 4. (a) Complex coordinate rotated eigenenergies $E_n(\theta)$ ($\theta = 0.16$), plotted as red circles. The light blue lines are rotated cuts. The black arrow shows the resonance pole (see the lower panel). (b) Complex coordinate rotation trajectories around the resonance energy. The different colors correspond to different sets of basis functions. The open circles are results calculated for values of θ incremented from 0 to 0.22 by 0.02. Each arrow indicates the direction of increasing θ .

The real part of $\langle r_{ij} \rangle$ gives the probable expectation value, and the imaginary part can be regarded as its uncertainty due to the finiteness of the lifetime of the resonance state [46–48]. Table II lists those mean distances for which the size of the resonance state is found to be similar to that of the bound state. It is found that $\langle r_{p,e^-} \rangle$ and $\langle r_{e^-,e^-} \rangle$ of the resonance state are slightly smaller than those of the bound state. On the other hand, $\langle r_{p,e^+} \rangle$ is slightly larger than that of the bound state, and $\langle r_{p,e^+} \rangle$ remains nearly unchanged. Thus, the transition from the bound state to the resonance state should be accompanied primarily by shrinkage of the electronic cloud but not by the positronic one.

C. Radiative dissociation rates

Now we evaluate the radiation spectrum according to Eq. (5) in both length and velocity gauges. Figure 5 displays

TABLE II. The real part of the expectation values of interparticle distance in the PsH bound state ($2,4S^o$) and resonance state ($2,4P^e$). The proton-electron mass ratio is set to $m_p/m_e = 1836.152\,673\,89$ [45]. The digit in parentheses denotes the uncertainty in the last digit obtained from the imaginary part of the expectation value.

	$\langle r_{p,e^-} \rangle$	$\langle r_{e^-,e^+} \rangle$	$\langle r_{p,e^+} \rangle$	$\langle r_{e^-,e^-} \rangle$	$\langle r_{p,(e^-e^+)} \rangle$
Bound state	8.894	12.74	14.28	14.05	10.01
Resonance state	7.45(7)	13.5(2)	14.2(2)	12.3(1)	9.1(1)

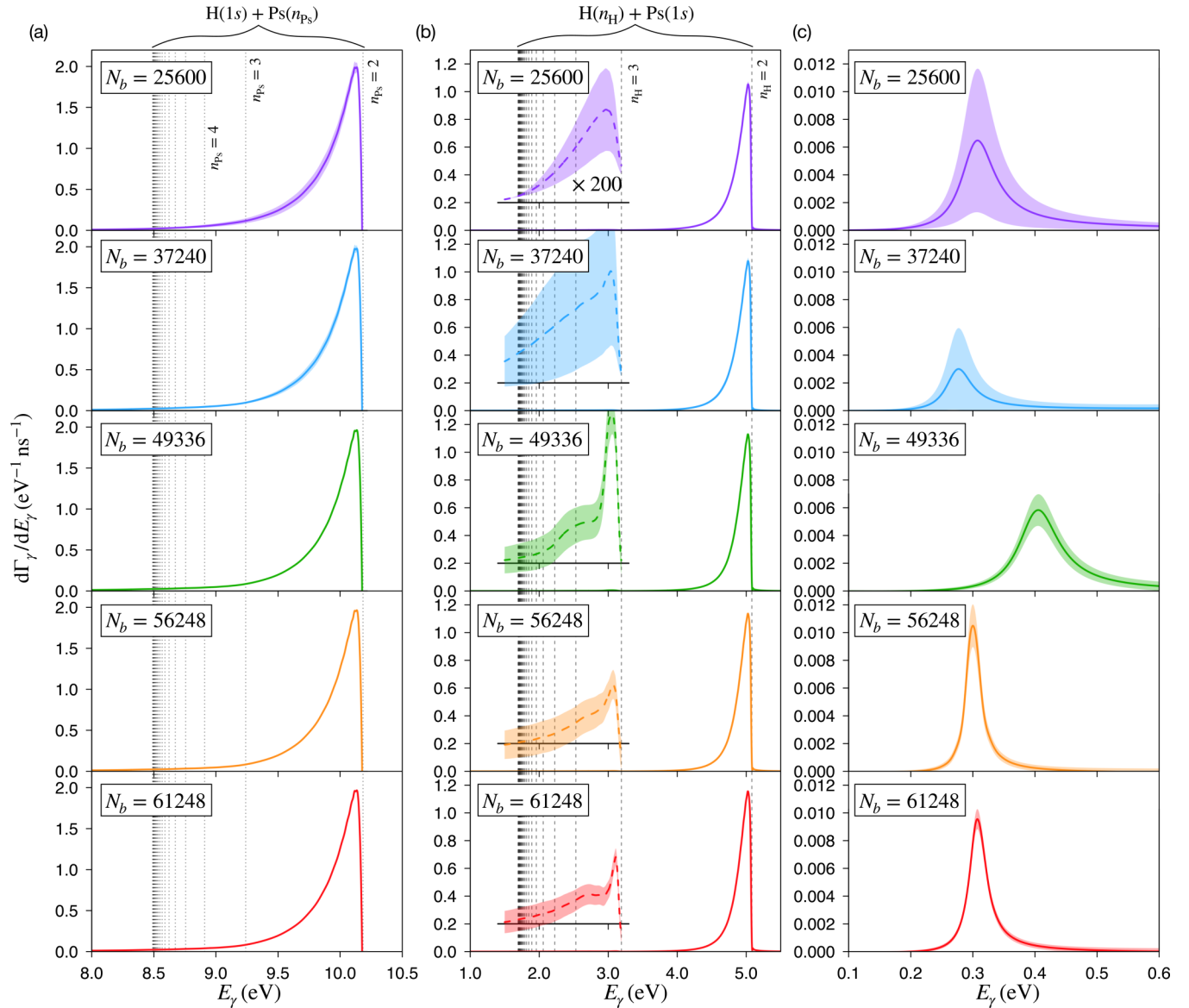


FIG. 5. Radiation spectra calculated by five different sets of basis functions. N_b denotes the total number of basis functions. The solid lines are the averaged results of the length- and velocity-gauge calculations; the shaded areas denote the discrepancy between them. (a) Energy range from 8.0 to 10.5 eV. The vertical dotted lines indicate the energy difference between E_i and the threshold energies of $H(1s) + Ps(n_{ps} \geq 2)$. (b) Energy range from 1.0 to 5.5 eV. The vertical dashed lines indicate the energy difference between E_i and the threshold energies of $H(n_H \geq 2) + Ps(1s)$. The insets show that part of the spectrum multiplied by 200. (c) Energy range from 0.1 to 0.6 eV.

$d\Gamma_\gamma/dE_\gamma$ against E_γ as obtained by five different sets of basis functions, with counts of $N_b = 25\,600$ with 2 arrangement channels, $N_b = 37\,240$ with 5 arrangement channels, $N_b = 49\,336$ with 12 arrangement channels, $N_b = 56\,248$ with 16 arrangement channels, and $N_b = 61\,248$ with 21 arrangement channels. In each of the calculations, 2400 pseudostates are included in the summation in Eq. (5). In the set of basis functions with $N_b = 61\,248$, $\psi_1(\theta)$ and $\psi_{2400}(\theta)$ correspond to $\text{Re}E_1(\theta) = -0.562\,166$ and $\text{Re}E_{2400}(\theta) = -0.024\,566$, respectively. It should be noted that the calculation results are unchanged against the number of pseudostates ≥ 2000 . The discrepancy between the length- and velocity-gauge calculations is indicated by the shaded areas, and their average is shown as solid lines. The maximum photon energy E_γ is 10.18 eV, which is close to the energy difference between

E_i and the lowest threshold energy of $H(1s) + Ps(2p)$. In general, the discrepancy between the length- and velocity-gauge calculations decreases as the number of basis functions increases.

The radiation spectrum has two notable peaks at $E_\gamma = 10.14$ eV and $E_\gamma = 5.02$ eV as well as small peaks at $E_\gamma = 3$ eV and $E_\gamma = 0.306$ eV. Figure 5(a) shows the highest peak, found at $E_\gamma = 10.14$ eV, which almost corresponds to the energy difference between E_i and the threshold energy of $H(1s) + Ps(2p)$. As there are no other dissociation channel in $E_\gamma > 9.23$ eV, this peak can be definitively attributed to the radiative dissociation into $H(1s) + Ps(2p)$. It can be seen that the five different sets of basis functions give well-converged results on the radiation spectrum in the energy range $8.0 < E_\gamma < 10.2$ eV. Moreover, both length- and velocity-gauge

TABLE III. Resonance energy E_r , width Γ_c , and lifetime $\tau_c = \Gamma_c^{-1}$ of $\text{PsH}(^{2,4}P^e)$ resonance state as calculated by the complex coordinate rotation method (CCRM) and Lorentzian fitting of the radiation spectrum.

Method	E_r (a.u.)	Γ_c (a.u.)	τ_c (ps)
Lorentzian fitting	-0.199 607	0.001 130	0.021 41
CCRM	-0.199 502	0.001 182	0.020 46

calculations give consistent results, affirming the accuracy of our calculation.

The second highest peak is at $E_\gamma = 5.02$ eV, as shown in Fig. 5(b). It is situated close to the energy difference between E_i and the threshold energy of $\text{H}(2p) + \text{Ps}(1s)$. Although this peak could in principle be contributed by the radiative dissociation into $\text{H}(1s) + \text{Ps}(n_{p_s} \geq 2)$ and the exact decomposition of these components is not possible, in light of the steep rise of this peak at the threshold energy, it can fairly be attributed to the radiation of the dissociation into $\text{H}(2p) + \text{Ps}(1s)$. As with the primary peak at $E_\gamma = 10.14$ eV, the five different sets of basis functions give well-converged results.

From previous work [44] and our discussion in Subsec. III A, $\text{PsH}(^{2,4}S^o)$ is considered to be a loosely bound state of $\text{H}(2p)$ and $\text{Ps}(2p)$. A radiation spectrum whose two highest peaks are attributable to the dissociation into $\text{H}(1s) + \text{Ps}(2p)$ and $\text{H}(2p) + \text{Ps}(1s)$ is consistent with this picture.

The energy transfer between $\text{H}(2p)$ and $\text{Ps}(2p)$ upon the spontaneous radiative dissociation would be an intriguing subject for investigation. The deexcitation energy of $\text{H}(2p)$ to $\text{H}(1s)$ is 0.375 a.u., which is sufficient to induce excitation of $\text{Ps}(2p)$, as its binding energy is 0.0625 a.u. Similarly, the energy gap of $\text{Ps}(2p)$ to $\text{Ps}(1s)$, 0.1875 a.u., is sufficient to excite $\text{H}(2p)$, whose binding energy is 0.125 a.u. Thus, in principle, there are branches resulting in $\text{H}(1s)$ and excited Ps or in excited H and ground-state Ps. However, in the tail of the primary peak [Fig. 5(a)], we did not observe any clear peak near the former threshold energies. In contrast, as can be seen in the insets of Fig. 5(b), there is a small but clear peak at $E_\gamma = 3$ eV, the threshold energy of $\text{H}(3p/3d) + \text{Ps}(1s)$. This suggests that the deexcitation energy of $\text{Ps}(2p \rightarrow 1s)$ tends to transfer to the $\text{H}(2p)$, not vice versa.

Figure 5(c) shows the peak found near $E_\gamma = 0.306$ eV. This peak can be attributed to the transition from $\text{PsH}(^{2,4}S^o)$ to the resonance state $\text{PsH}(^{2,4}P^e)$ investigated in Subsec. III B. As $\text{PsH}(^{2,4}S^o)$ is truly a bound state unless it couples with the radiation field, the spectral shape of the transition to the resonance state $\text{PsH}(^{2,4}P^e)$ should be characterized by the resonance energy E_r and width Γ_c of $\text{PsH}(^{2,4}P^e)$.

In the absence of the background phase, the spectral shape can be analyzed by a Lorentzian function as

$$\frac{d\Gamma_\gamma}{dE_\gamma} = A \frac{\Gamma_c/2}{(E_\gamma - E_i + E_r)^2 + \Gamma_c^2/4}, \quad (15)$$

where A is a constant. Note that Γ_c is the nonradiative dissociation rate of $\text{PsH}(^{2,4}P^e)$. We fitted the radiation spectrum by Eq. (15) with free parameters E_r , Γ_c , and A . The values obtained for E_r and Γ_c are listed in Table III. They are in good agreement with those calculated by the complex coordinate

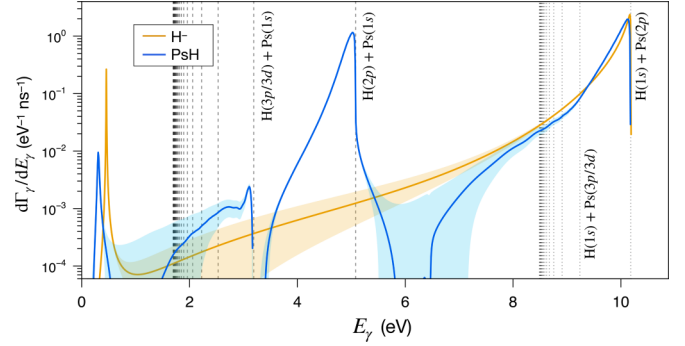


FIG. 6. Blue line, radiation spectrum of $\text{PsH}(^{2,4}S^o)$; orange line, that of $\text{H}^-(^3P^e)$. The solid lines indicate the average of the velocity-gauge and length-gauge calculation results, and the shaded areas indicate their discrepancy.

rotation method shown in Fig. 4(b). Therefore, the peak at $E_\gamma = 0.306$ eV is undoubtedly attributable to the transition to the $\text{PsH}(^{2,4}P^e)$ resonance state.

Although the amplitude of this peak is smaller than those of the primary and secondary peaks at $E_\gamma = 10.14$ and 5.02 eV, the transition to the resonance state embedded in the $^{2,4}P^e$ continuum has features that differ from those of radiative dissociation into the nonresonant continuum. The $^{2,4}P^e$ resonance state has a lifetime of 0.02 ps and is located far above the $p + e^- + \text{Ps}(1s)$ threshold energy. As the center of mass of the system is located almost precisely at the proton, the nonradiative decay of the $^{2,4}P^e$ resonance state may produce $\text{Ps}(2p)$ with 9.9 eV kinetic energy and $\text{Ps}(1s)$ with 4.8 eV kinetic energy. This is in contrast to the radiative dissociation into the nonresonant continuum state of $\text{H}(1s) + \text{Ps}(2p)$ and $\text{H}(2p) + \text{Ps}(1s)$, in which most of the deexcitation energy is carried away by the photon, thereby producing the slow Ps.

D. Branch estimation and comparison with $\text{H}^-(^3P^e)$ radiative dissociation

Figure 6 shows a gross view of the radiation spectrum of $\text{PsH}(^{2,4}S^o)$ together with that of $\text{H}^-(^3P^e)$ calculated in a framework similar to that described for PsH. For calculation of the $\text{H}^-(^3P^e)$ spectrum, we used 3904 basis functions for the bound state, reproducing the binding energy of the best variational calculation [49] to greater than six-digit precision. As the $\text{H}^-(^3P^e)$ bound state is located just below the $\text{H}(2p) + e^-$ dissociation threshold energy, the maximum photon energy is 10.19 eV, which is very close to the maximum photon energy from $\text{PsH}(^{2,4}S^o)$.

The spectrum of $\text{H}^-(^3P^e)$ has two clear peaks, at $E_\gamma = 10.17$ and 0.456 eV. The higher energy peak corresponds to the radiative dissociation into the $\text{H}(1s) + e^-$ continuum, and the lesser one corresponds to the radiative transition into the $2s2p$ resonance state of $^3P^o$ [36]. The spectral shape around the higher energy peak resembles that of $\text{PsH}(^{2,4}S^o)$. The half width at half maximum of the highest peak of $\text{PsH}(^{2,4}S^o)$ is slightly greater than that of $\text{H}^-(^3P^e)$, which means that the deexcitation energy is more effectively transferred to kinetic energy of the relative motion of the dissociation fragments. Although $\text{PsH}(^{2,4}S^o)$ would have the structure of a loosely bound state consisting of $\text{H}(2p)$ and $\text{Ps}(2p)$, it can also be

TABLE IV. Summary of radiative transition rates for $H(2p)$ and $Ps(2p)$, $H^-(^3P^e)$, and $PsH(^{2,4}S^o)$. The digit in parentheses denotes the uncertainty estimated by the discrepancy between the velocity- and length-gauge calculations.

System	Γ_γ (s^{-1})	τ_γ (ns)
$H(2p) \rightarrow H(1s)$	6.26×10^8	1.60
$Ps(2p) \rightarrow Ps(1s)$	3.13×10^8	3.19
$H^-(^3P^e)$		
$\rightarrow H^-(^3P^o)$	2.4×10^6	4.2×10^2
$\rightarrow H(1s) + e^-$	5.80×10^8	1.72
Total	5.82×10^8	1.72
Total [35]	5.77×10^8	
$PsH(^{2,4}S^o)$		
$\rightarrow PsH(^{2,4}P^e)$	4.6×10^5	2.2×10^3
\rightarrow excited H + Ps(1s)	$2.71(1) \times 10^8$	3.69(3)
$\rightarrow H(1s) +$ excited Ps	$6.4(1) \times 10^8$	1.57(4)
Total	$9.1(2) \times 10^8$	1.10(3)

considered as a bound state between $H^-(^3P^e)$ and the positron in the p orbital. As shown in the $p-e^-$ correlation function in Fig. 3(a), the electrons of the $PsH(^{2,4}S^o)$ bound state are closer to the proton than those of $H^-(^3P^e)$. As the $p-e^-$ mean distance of $H^-(^3P^e)$, $\langle r_{p,e^-} \rangle = 11.66$, is greater than that of $PsH(^{2,4}S^o)$, $\langle r_{p,e^-} \rangle = 8.894$, one can expect tighter interaction between the dissociation fragments. Therefore, the widening of the radiation spectrum for $PsH(^{2,4}S^o)$ is convincing.

$H^-(^3P^e)$ also exhibits the bound–resonance transition peak, which is consistent with Ref. [36]. There is a resemblance in the resonance peaks between $PsH(^{2,4}S^o)$ and $H^-(^3P^e)$, though the peak height in $H^-(^3P^e)$ is greater than that in $PsH(^{2,4}S^o)$.

Although the present calculation does not distinguish the final state fragments and consequently does not rigorously determine the branching ratio for the spontaneous radiative dissociation, we estimate the branching ratio based on the integration of the radiation spectrum by utilizing the large discrepancy of the threshold energies of $H(1s) + Ps(n_{Ps} \geq 2)$ and $H(n_H \geq 2) + Ps(1s)$.

For $H^-(^3P^e)$, the rate of transition to the $2s2p$ resonance state of $^3P^o$ is calculated by integration of the fitted Lorentzian function. The total radiative dissociation rate, including the transition to the resonance state, is calculated by integration of $d\Gamma_\gamma/dE_\gamma$ over $0 \leq E_\gamma \leq 10.19$ eV. The radiative dissociation rate to the nonresonant $H(1s) + e^-$ continuum is obtained by subtracting the rate of transition to the resonance state from the total rate. Similarly for $PsH(^{2,4}S^o)$, the rate of transition to the $^{2,4}P^e$ resonance state is calculated by integration of the fitted Lorentzian function. The total rate is given by the integration of $d\Gamma_\gamma/dE_\gamma$ over the entire energy range. The rates of radiative dissociation resulting in $H(1s) +$ excited Ps and excited H + Ps(1s) are approximated by integrating $d\Gamma_\gamma/dE_\gamma$ over $5.08 \leq E_\gamma \leq 10.18$ and $0 \leq E_\gamma \leq 5.08$ eV, respectively.

These estimated values are summarized in Table IV along with the spontaneous deexcitation rates for $H(2p)$ and $Ps(2p)$.

The total radiative dissociation rate for $H^-(^3P^e)$, $5.82 \times 10^8 s^{-1}$, is comparable to the one previously reported, $5.77 \times 10^8 s^{-1}$ [35]. The contribution of the bound–resonance transition is 0.4% of the total rate. For $PsH(^{2,4}S^o)$, the total rate is

$9.1(2) \times 10^8 s^{-1}$, which is greater than that of $H^-(^3P^e)$. The contribution of the bound–resonance transition is 0.05% of the total rate. The radiative dissociation resulting in the $H(1s)$ fragment has a rate of $6.4(1) \times 10^8 s^{-1}$, which is also greater than that for $H^-(^3P^e)$ and is comparable to the rate of spontaneous radiative deexcitation of $H(2p)$. The rate resulting in the $Ps(1s)$ fragment, in turn, is $2.71(1) \times 10^8 s^{-1}$, which is slightly less than the spontaneous radiative transition rate for $Ps(2p)$. These theoretical observations are consistent with the structural analyses above.

IV. CONCLUSION

We have reported the spontaneous radiative dissociation spectrum of the second bound state of $PsH(^{2,4}S^o)$ based on the calculation utilizing complex coordinate rotated wave functions. The accuracy of the results were carefully investigated by their convergence against the choice of basis functions and the choice of length and velocity gauges.

$PsH(^{2,4}S^o)$ predominantly undergoes dissociation with emission of a photon whose radiation spectrum peaks at 10.14 and 5.02 eV. The former peak is attributable to transition to the continuum states of $H(1s) + Ps(2p)$, and the latter one mainly to those of $H(2p) + Ps(1s)$. We also reported that the radiative dissociation spectrum of $PsH(^{2,4}S^o)$ has aspects similar to those of $H^-(^3P^e)$. In particular, the radiation resulting in the $H(1s)$ fragment has almost the same spectral shape. Both the rate resulting in the $H(1s)$ fragment and that resulting in the $Ps(1s)$ fragment are close to those of $2p \rightarrow 1s$ transition rates, which suggests that $PsH(^{2,4}S^o)$ is a loosely bound state of $H(2p)$ and $Ps(2p)$. The total rate of the spontaneous radiative dissociation is calculated to be $9.1(2) \times 10^8 s^{-1}$.

In the present calculation, we do not consider the annihilation branch; however, given that the structure of $PsH(^{2,4}S^o)$ can be considered as the loosely bound state of $H(2p)$ and $Ps(2p)$, the annihilation rate would be similar to that of $Ps(2p)$. In the literature [50,51], the 2γ annihilation lifetime of $Ps(2p)$ is known to exceed 100 μs , corresponding to the rate of $\lesssim 10^4 s^{-1}$ which is smaller than the radiative transition rate into the resonance state identified in the present work.

The radiative transition to the resonance state of $^{2,4}P^e$, whose lifetime against the nonradiative dissociation is 0.02 ps, is found to make a small contribution to the total rate of the radiative dissociation. The resonance state may emit 9.9 eV $Ps(2p)$ in its short lifetime, which could pave the way for future experiments to observe $PsH(^{2,4}S^o)$. Besides, the reverse process, namely the photon absorption of the $^{2,4}P^e$ resonance state resulting in the $PsH(^{2,4}S^o)$ bound state, might also contribute to the stellar spectrum involving the excited H and/or Ps.

ACKNOWLEDGMENTS

This work was financially supported by JSPS KAKENHI for Grants No. 18H05407, No. JP20K14381, and No. JP21H00115. The computation was conducted on the supercomputers ITO at Kyushu University, FLOW at Nagoya University, and HOKUSAI at RIKEN.

- [1] S. Chandrasekhar, *Rev. Mod. Phys.* **16**, 301 (1944).
- [2] G. B. Field, W. B. Somerville, and K. Dressler, *Annu. Rev. Astron. Astrophys.* **4**, 207 (1966).
- [3] J. M. Shull and S. Beckwith, *Annu. Rev. Astron. Astrophys.* **20**, 163 (1982).
- [4] M. Gerin, D. A. Neufeld, and J. R. Goicoechea, *Annu. Rev. Astron. Astrophys.* **54**, 181 (2016).
- [5] T. J. Millar, C. Walsh, and T. A. Field, *Chem. Rev.* **117**, 1765 (2017).
- [6] R. Wildt, *Astrophys. J.* **89**, 295 (1939).
- [7] R. Wildt, *Astrophys. J.* **90**, 611 (1939).
- [8] S. Chandrasekhar, *Astrophys. J.* **102**, 223 (1945).
- [9] S. Chandrasekhar and D. D. Elbert, *Astrophys. J.* **128**, 633 (1958).
- [10] V. L. Jacobs, A. K. Bhatia, and A. Temkin, *Astrophys. J.* **242**, 1278 (1980).
- [11] A. M. Frolov, *J. Phys. B: At. Mol. Opt. Phys.* **37**, 853 (2004).
- [12] S. B. Zhang, J. G. Wang, R. K. Janev, Y. Z. Qu, and X. J. Chen, *Phys. Rev. A* **81**, 065402 (2010).
- [13] A. Ghoshal and Y. K. Ho, *Phys. Rev. E* **81**, 016403 (2010).
- [14] B. M. McLaughlin, P. C. Stancil, H. R. Sadeghpour, and R. C. Forrey, *J. Phys. B: At. Mol. Opt. Phys.* **50**, 114001 (2017).
- [15] E. Holøien, *J. Chem. Phys.* **33**, 301 (1960).
- [16] E. Holøien, *Phys. Norvegica* **1**, 51 (1961).
- [17] G. W. F. Drake, *Phys. Rev. Lett.* **24**, 126 (1970).
- [18] F. Martín, *J. Phys. B: At. Mol. Opt. Phys.* **32**, L181 (1999).
- [19] J. Komasa, *Phys. Chem. Chem. Phys.* **10**, 3383 (2008).
- [20] F. Argoubi, S. Bezzaouia, H. Oueslati, M. Telmini, and C. Jungen, *Phys. Rev. A* **83**, 052504 (2011).
- [21] J. A. Wheeler, *Ann. New York Ac. Sci.* **48**, 219 (1946).
- [22] A. Ore, *Phys. Rev.* **83**, 665 (1951).
- [23] C. F. Lebeda and D. M. Schrader, *Phys. Rev.* **178**, 24 (1969).
- [24] K. Strasburger and H. Chojnacki, *Chem. Phys. Lett.* **241**, 485 (1995).
- [25] A. M. Frolov and V. H. Smith, *Phys. Rev. A* **55**, 2662 (1997).
- [26] J. Usukura, K. Varga, and Y. Suzuki, *Phys. Rev. A* **58**, 1918 (1998).
- [27] C. L. Sech and B. Silvi, *Chem. Phys.* **236**, 77 (1998).
- [28] Z.-C. Yan and Y. K. Ho, *Phys. Rev. A* **59**, 2697 (1999).
- [29] M. Mella, G. Morosi, and D. Bressanini, *J. Chem. Phys.* **111**, 108 (1999).
- [30] S. L. Saito, *Nucl. Instrum. Methods Phys. Res., Sect. B* **171**, 60 (2000).
- [31] S. L. Saito, *J. Chem. Phys.* **118**, 1714 (2003).
- [32] S. Bubin and K. Varga, *Phys. Rev. A* **84**, 012509 (2011).
- [33] N. Prantzios, C. Boehm, A. M. Bykov, R. Diehl, K. Ferrière, N. Guessoum, P. Jean, J. Knoedlseder, A. Marcowith, I. V. Moskalenko, A. Strong, and G. Weidenspointner, *Rev. Mod. Phys.* **83**, 1001 (2011).
- [34] J. Mitroy and M. W. J. Bromley, *Phys. Rev. Lett.* **98**, 063401 (2007).
- [35] G. W. F. Drake, *Astrophys. J.* **184**, 145 (1973).
- [36] V. L. Jacobs, A. K. Bhatia, and A. Temkin, *Astrophys. J.* **191**, 785 (1974).
- [37] Y. Ho, *Phys. Rep.* **99**, 1 (1983).
- [38] T. N. Rescigno and V. McKoy, *Phys. Rev. A* **12**, 522 (1975).
- [39] A. Buchleitner, B. Gremaud, and D. Delande, *J. Phys. B: At. Mol. Opt. Phys.* **27**, 2663 (1994).
- [40] S. Kilic, J.-P. Karr, and L. Hilico, *Phys. Rev. A* **70**, 042506 (2004).
- [41] D. A. Varshalovich, A. N. Moskalev, and V. K. Khersonskii, *Quantum Theory of Angular Momentum* (World Scientific, Singapore, 1988).
- [42] E. Hiyama, Y. Kino, and M. Kamimura, *Prog. Part. Nucl. Phys.* **51**, 223 (2003).
- [43] E. Hiyama, *Prog. Theo. Exp. Phys.* **2012**, 01A204 (2012).
- [44] M. W. J. Bromley, J. Mitroy, and K. Varga, *Phys. Rev. A* **75**, 062505 (2007).
- [45] E. Tiesinga, P. J. Mohr, D. B. Newell, and B. N. Taylor, The 2018 CODATA recommended values of the fundamental physical constants (web version 8.1), National Institute of Standards and Technology, Gaithersburg, <http://physics.nist.gov/constants>.
- [46] T. Berggren, *Nucl. Phys. A* **109**, 265 (1968).
- [47] A. Bürgers and J.-M. Rost, *J. Phys. B: At. Mol. Opt. Phys.* **29**, 3825 (1996).
- [48] G. Papadimitriou, *Few-Body Syst.* **57**, 833 (2016).
- [49] S. Kar and Y. K. Ho, *J. Phys. B: At. Mol. Opt. Phys.* **42**, 185005 (2009).
- [50] A. Alekseev, *Zh. Eksp. Teor. Fiz.* **34**, 1195 (1958) [*Sov. Phys. JETP* **7**, 826 (1958)].
- [51] A. Sen and Z. K. Silagadze, *Can. J. Phys.* **97**, 693 (2019).